PCCP

PAPER

View Article Online
View Journal | View Issue

Cite this: *Phys. Chem. Chem. Phys.*, 2025, **27**, 20313

Vibrational signature of $1^1B_u^+$ and hot $2^1A_g^-$ excited states of carotenoids revisited by femtosecond stimulated Raman spectroscopy

Petra Chrupková,[ab] Andrej Hovan,[ac] Michal Koblížek,[d] Alastair T. Gardiner,[d] Tomáš Polívka[b] and Miroslav Kloz*[a]

Received 16th July 2025,
Accepted 3rd September 2025

DOI: 10.1039/d5cp02711j

rsc.li/pccp

The significance of carotenoids in biological systems cannot be overstated. Their functionality largely arises from unique excited-state dynamics, where photon absorption promotes the molecule to the optically allowed $1^1B_u^+$ state (conventionally S_2), which rapidly decays to the optically forbidden $2^1A_g^-$ state (S_1). While the vibrational signature of the S_1 state is well established, that of the initial S_2 state has remained elusive. In this work, we identify a consistent S_2-state vibrational signature across five different carotenoids and explain the challenges in isolating this signature. Resonance conditions in the near infrared region cause the S_2 signal to appear as a complex superposition of contributions from stimulated emission to the ground state, excited-state absorption (S_2 to S_m), and vibrationally inverted S_1 signals. This results in a mix of positive and negative features that are not trivial to disentangle. After careful analysis, we isolated the genuine S_2 signature, characterized by a C=C stretch near 1600 cm^{-1} and a C–C stretch near 1350 cm^{-1}. The remaining signals originate from the ground or S_1 states but are virtually inseparable from the FSRS signal on S_2-state timescales. Our findings resolve a long-standing spectroscopic challenge and clarify the early excited-state dynamics of carotenoids.

Introduction

Efforts to capture ultrafast vibrational dynamics in excited carotenoids closely parallel the development of ultrafast Raman spectroscopy. Carotenoids are excellent Raman scatterers but exhibit very weak fluorescence, making them ideal systems for evaluating time-resolved Raman techniques. Their biological significance further strengthens their relevance in this context. Raman spectra of carotenoids are quite simple and dominated by three well isolated bands: C=C stretching (ν_1 mode) at 1510–1530 cm^{-1}, C–C stretching (ν_2 mode) at 1150–1160 cm^{-1}, and CH_3 rocking (ν_3 mode) at 1000–1010 cm^{-1}.[1] Other modes are not to be discussed in this work although some of them may be relevant for understanding carotenoid dynamic in proteins, in particular the C–H out-of-plane bending sometimes shortened as "hoop" (ν_4 mode) around 960 cm^{-1} that becomes Raman active if the polyene backbone gets twisted. Early experiments using traditional non-coherent Raman scattering with picosecond laser pulses revealed that the lowest excited state of carotenoids, the so-called S_1, which is a common name for the $2^1A_g^-$ state of linear polyenes,[2] representing the lowest lying excited state (ES) in case of carotenoids, exhibits an upshifted C=C stretch vibration.[3,4] In β-carotene (Bcar), this mode shifts from approximately 1526 cm^{-1} in the ground state (GS) to around 1790 cm^{-1} in the S_1[3,5–8] (hereafter, S_1 is a synonym for the $2^1A_g^-$ state without necessary implying its ordering in the excited state manifold), with slight variations among different carotenoids.[9]

These experiments also showed a notable absence of the S_1 Raman signature in the anti-Stokes region,[10] which will be commented in the Discussion section. Currently, the most established model of carotenoid photodynamic assumes that the S_1 state is never directly populated by a single photon absorption,[11] but it is populated from another state, commonly referred to as S_2, corresponding to the $1^1B_u^+$ state of carotenoids (hereafter, S_2 is a synonym for the $1^1B_u^+$ state without necessary implying its ordering on excited state manifold).[2,12] This state is responsible for the HOMO–LUMO transition and in picosecond spontaneous Raman experiments it exhibited no observable Raman signature.[8] This was attributed to its ultrashort lifetime, approximately 180 femtoseconds in Bcar (and even shorter in polyenes with a conjugation length exceeding that of Bcar[12]), which was considered too brief to be resolved using

[a] *The Extreme Light Infrastructure ERIC, ELI Beamlines Facility, Za Radnicí 835, Dolní Břežany, Czech Republic. E-mail: miroslav.kloz@eli-beams.eu*
[b] *Department of Physics, Faculty of Science, University of South Bohemia, Branišovská 1760, 370 05 České Budějovice, Czech Republic*
[c] *Department of Biophysics, Faculty of Science, P.J. Šafárik University in Košice, Jesenná 5, 041 54, Košice, Slovakia*
[d] *Laboratory of Anoxygenic Phototrophs, Institute of Microbiology, Czech Academy of Sciences, 379 81 Třeboň, Czech Republic*

picosecond Raman excitation pulses. The assignment of the S_2 lifetime was instead accomplished through transient absorption (TA) spectroscopy,[13] femtosecond Kerr gate fluorescence spectroscopy,[14] and fluorescence up-conversion[12] which probes stimulated emission (SE) from the S_2 state—a feature that is virtually absent in the S_1 state.[15,16] In both TA and Kerr gate experiments, the instrument response function (IRF) is, within certain limits, governed by the duration of the actinic pulse that initiates the photochemical process.

Pulses with durations below 50 fs are now readily available, enabling the resolution of such ultrafast dynamics. In time-resolved Raman spectroscopy, however, the situation is more complex. Owing to the time–energy uncertainty inherent to spontaneous Raman scattering, a Raman excitation pulse with a Gaussian full width at half maximum (FWHM) of 15 cm^{-1} corresponds to a temporal duration of approximately 1 ps. As a result, even if the reaction is initiated by a femtosecond pulse and a significant transient population of the S_2 state is achieved, structural information specific to S_2—as compared to S_1—would be temporally broadened and effectively smeared out.[10] This limitation was eventually overcome with the resurgence of Femtosecond Stimulated Raman Spectroscopy (FSRS),[17] enabling vibration-sensitive measurements on ultrafast timescales. Since the advent of FSRS, numerous studies have sought to establish the vibrational fingerprint of the S_2 state, but results remain inconsistent.[5,18,19] Over 25 years since the method's establishment, a consensus on the Raman signature of this state is still lacking—despite its importance in understanding FSRS signals from light-harvesting complexes and related systems such as retinal proteins that also contain $1^1B_u^+$ and $2^1A_g^-$ states in their excited state manifold (S_1/S_2 notation is not used for retinal proteins consistently with carotenoids).[20]

In this study, we seek to identify the key factors that have made assignment of the S_2 state's Raman signature more challenging than that of the S_1 state. To support our analysis, we examine a series of structurally related carotenoids—neurosporene (Neu), β-carotene (Bcar), spheroidene (Spn), lycopene (Lyc), and spirilloxanthin (Spx). The structures and conjugation lengths of these carotenoids are presented in Fig. 1. Although Raman signatures of the S_2 state exhibit considerable quantitative variation across these compounds, their qualitative spectral features are consistently reproduced, underscoring the internal coherence of the observed phenomena. Alongside presenting our assignment of the S_2 Raman signature, we also propose a comprehensive interpretation of its spectral characteristics. To establish this framework, we first provide a concise overview of the principles and specific considerations relevant to FSRS spectroscopy.

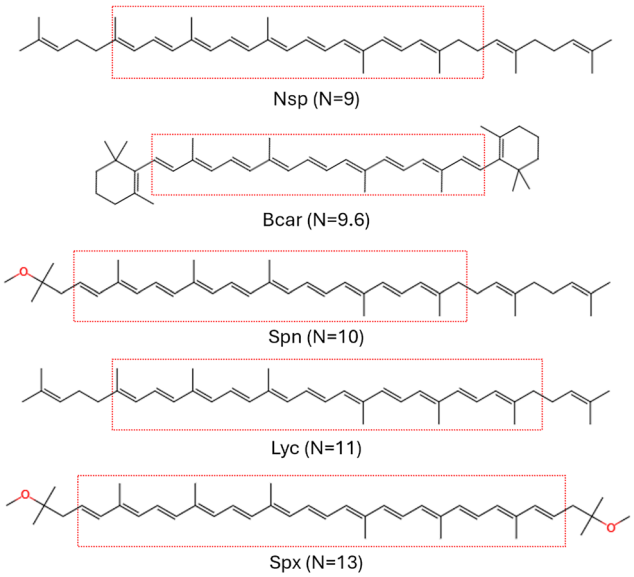

Fig. 1 Molecular structures of neurosporene, β-carotene, spheroidene, lycopene and spirilloxanthin. The red rectangles show the conjugation length of the particular carotenoid.

Fundamentals of FSRS

Stimulated Raman spectroscopy is a coherent four-wave mixing process.[21] Unlike spontaneous Raman scattering, where inelastic scattering of a monochromatic pump generates a frequency-shifted signal, FSRS involves a broadband probe pulse (Pr) whose transmission spectrum is modified due to interactions with a narrowband Raman pump (Rp) *via* the sample's third-order polarizability. While a full theoretical treatment is beyond the scope of this work, several features of FSRS are critical to understanding the phenomena discussed here:

Temporal resolution beyond time–energy constraints

FSRS is not limited by the energy–time uncertainty principle in the same way as spontaneous Raman scattering. Vibrational coherence that is probed by FSRS is generated *via* cross-correlation between the Rp and Pr pulses, and in time-resolved experiments, also with an actinic pump (Pu) that initiates the photoreaction. With modern femtosecond lasers, sub-100 fs pump–probe cross-correlations are routinely achievable, making it possible to probe even very short-lived states like carotenoid S_2.[22] Nevertheless, extraction of meaningful vibrational information still requires deconvolution from the IRF that include artifacts that are for FSRS more complex than in case of TA, but luckily significant progress in this direction has been recently achieved.[23,24]

Spectral signatures of short-lived states

FSRS can capture Raman signals from states with lifetimes as short as tens of femtoseconds.[22] However, the resulting signal is a convolution of the vibrational dephasing dynamics and the temporal profile of the Raman pump. Rapid vibration decoherence convoluted by short lifetime of the S_2 state inherently produces broad spectral features, even with a narrowband Rp. If the vibrational frequency evolves during decoherence, dispersive line shapes may appear.[25] For this reason, it is important to consider that vibrational signatures of states with approximately 100 fs duration will look different from what is

typically observed for a state with lifetime exceeding the vibrational decoherence.

Stokes *versus* anti-Stokes in FSRS

From this point on we denote as a Stokes process the phenomenon where Raman scattering excites the molecular vibration, while an anti-Stokes process is defined as the phenomenon where Raman scattering extracts vibrational energy from the molecule. In spontaneous Raman scattering, the Stokes process is strictly observed on the low energy side of the Rp wavelength and an anti-Stokes process at the high energy side, respectively, and adhere strictly to energy conservation laws in a sense that the high energy side (often called the anti-Stokes side) contains only signals from hot states. In FSRS, however, both Stokes and anti-Stokes fields are present at intensities above the vacuum level, rendering the distinction between the two processes. The vacuum field is capable of inducing de-excitation but cannot provide excitation, which imposes the aforementioned limitations for Stokes and anti-Stokes processes in spontaneous Raman scattering. However, when a real probe field is present, the Stokes field becomes capable of both excitation and de-excitation. Therefore, beating between the Rp and Pr fields at energy difference matching the molecular vibration can, both in the high and low energy side of the Rp pulse, lead to either excitation or de-excitation of the molecular vibrations depending on actual resonance conditions and molecular state.[26] Moreover, due to the Franck–Condon principle, electronically excited states are often populated in vibrationally hot configurations. As a result, both the low and high energy side bands may contain mixed contributions from Stokes and anti-Stokes processes during the early femtoseconds following excitation. In essence, both spectral regions in FSRS are influenced by processes traditionally labeled as Stokes and anti-Stokes. In this study, only the low energy side spectra are presented, primarily for clarity and simplicity. Nevertheless, it is important to recognize that these signals inherently include contributions from both Stokes and anti-Stokes processes—a critical consideration when analyzing the dynamics of the S_2 state and early S_1 state.

Resonance effects in FSRS

Resonance with excited-state absorption (ESA) or SE can significantly influence both the intensity and line shape of FSRS signals.[26,27] In the context of the results presented here, several principles are particularly important to consider. On the low energy side, resonance with ESA generally enhances the signal intensity without substantially distorting its spectral shape. In contrast, on the high energy side, such resonance can introduce dispersive distortions or even lead to an inversion of the spectral feature's sign.[28] When the FSRS signal is resonant with SE rather than with ESA, the behavior is reversed: the high energy side signal tends to exhibit straightforward enhancement, whereas the low energy side signal may become dispersive or even negative. In this work, we define a ''positive'' FSRS signal as one corresponding to a gain in the probe field, and a ''negative'' signal as one indicating absorption of the probe field. Dispersive features represent a combination of both gain and absorption contributions. These resonance-dependent effects imply that for excited states exhibiting both ESA and SE, such as the S_2 state of carotenoids, the FSRS spectrum will appear as a superposition of positive and negative features. Interpreting such complex spectra requires careful attention to the underlying resonance conditions; any assumption that peaks must be strictly positive or negative may lead to misinterpretation. This interpretation is supported by TA experiments,[29] which have demonstrated that the S_2 state displays both broad ESA and SE features. Consequently, its FSRS spectrum is expected to reflect this duality in a nontrivial manner.

Methods

FSRS and TA measurements were performed using a Ti:sapphire-based laser system. The original laser output centered at 780 nm was used as the Raman pump, and the actinic pump energy was set to 200 nJ in all cases. Five carotenoids were studied: Neu, Bcar, Spn, Lyc, and Spx. The excitation wavelengths were chosen to match the 0-0 vibronic transition in the absorption spectrum of each compound: Neu – 475 nm, Bcar – 475 nm, Spn – 492 nm, Lyc – 513 nm, and Spx – 522 nm. All samples were prepared to achieve an optical density of 1.5–1.7 at the respective excitation wavelength and were circulated through a 1 mm pathlength flow cuvette with a total sample volume of 1.5 mL to minimize photodegradation. Bcar was dissolved in carbon tetrachloride (CCl_4) to benefit from its broad Raman-silent region in the 1200–1900 cm^{-1} range. Lyc was dissolved in tetrahydrofuran (THF), while Neu, Spn, and Spx were dissolved in cyclohexane. The source and purity of all carotenoids, as well as a detailed description of the experimental station and pulse generation scheme, are provided in the Methods section of the SI.

To ensure data integrity, all spectra were subjected to rigorous baseline correction, as detailed in the SI (Section: Background subtraction). The correction method employed is based on a neural network model, designed to exclude spectral regions exhibiting excited-state dynamics from the baseline fitting process.[30] This strategy prevents artificial distortions in the spectral data. Previous work has shown that this neural network approach yields more reliable results than conventional methods such as polynomial fitting or smoothed data subtraction.[28] Furthermore, data recorded on Bcar and Lyc are acquired with more detailed time sampling and data are corrected for spurious solvent GS signal. The data from other carotenoids (Neu, Spn and Spx) are presented as direct baseline corrected transient FSRS, that means a direct difference between Pu-on and Pu-off FSRS signals. Such signal in general contains spurious GS bleach of all GS modes. In the case of Bcar, the absence of overlapping solvent features enabled a responsible subtraction of ground-state signals making this dataset comprise almost entirely of pure excited state FSRS signal. For the other carotenoids, subtracting a scaled ground-state spectrum would introduce residual artifacts as solvent

and carotenoids GS bleaches differently in excited sample, potentially leading to misinterpretation.[31] This is particularly critical for negative features associated with the S_2 state. Special care was taken to verify that for Bcar these negative signals represent genuine excited-state contributions rather than artifacts from overlapping positive features.

Results

The experimental results central to this study are presented in Fig. 2, which displays time-resolved FSRS spectra capturing the excited-state vibrational dynamics of a series of carotenoids. These molecules are arranged according to increasing effective conjugation length, defined as the number of conjugated double bonds along the polyene backbone: Neu (n = 9), Bcar (n = 9.6), Spn (n = 10), Lyc (n = 11), and Spx (n = 13). The non-integer conjugation length assigned to Bcar arises from its terminal β-rings, which contribute only partially to the conjugated system. This value is inferred from spectroscopic parameters extrapolated from fully linear carotenoids.[1,15] GS absorption spectra together with their fs TA can be found in literature.[5,9,13,32,33] For readers interested in further detail, full time-resolved Raman spectra for individual carotenoids are provided in the SI, Fig. S3–S7. In Fig. 2, each column presents dynamics associated predominantly with one key dynamic process. The first column captures the initial formation of the S_2 excited state; the second column illustrates the formation and vibrational cooling of the S_1 state; and the third column represents the final relaxation to the ground state. The spectra of Neu, Spn and Spx were measured in cyclohexane, Lyc in THF and Bcar in CCl_4. Although Bcar has been extensively studied in cyclohexane as well, one of the objectives of this work was to investigate its vibrational dynamics in a solvent that does not spectrally interfere with carotenoid vibrational modes. Therefore, Bcar was measured in CCl_4, which enables the acquisition of cleaner FSRS spectra by minimizing solvent-induced artifacts. Unfortunately, only Bcar was successfully measured in this solvent. As discussed later, no significant solvent-dependent differences in FSRS dynamics were observed, provided that unobstructed spectral regions are compared. However, the extent of spectral regions affected by solvent artifacts varies considerably between individual datasets.

This study focuses specifically on the assignment of the C=C stretching modes, which are well isolated from both solvent-induced features and ground-state vibrational bands in all experiments discussed. As such, their analysis can be considered effectively solvent-independent. In the case of the ground-state bleach, the dataset for Bcar is considered the most representative.

It is known that the S_1 state also exhibits minor contributions from C–C stretching modes. These modes are significantly less prominent in the excited state than the C=C modes but will be mentioned when they are clearly resolved and relevant to the discussion. Nevertheless, their assignment is inherently more limited, as C–C mode signals are more directly affected by solvent-related obfuscation, similar to GS bleach signals.

The time axes in the individual panels in Fig. 2 are not uniform for all carotenoids but were adapted to optimally capture the relevant dynamics of photophysical transitions in each. This approach reflects the well-established trend that both S_2 and S_1 excited-state lifetimes including cooling dynamics decrease with increasing conjugation length.[34,35] The time windows for each dataset were therefore tailored to encompass the S_2 to S_1 internal conversion and subsequent relaxation to the ground state specific to each carotenoid to enhance visualization of signatures associated with given state. For details of actual time evolution see Fig. 3 visualizing absolute S_2 and S_1 excited-state dynamics.

S_2 state

Identifying the spectral signature of the S_2 state is a central objective of this work and therefore warrants detailed attention. Across all studied carotenoids, three distinct components are consistently observed within the S_2-state lifetime (Fig. 2, left column). The first feature is a spectrally broad negative signal that overlaps with GS vibrational regions mentioned in the Introduction ($\sim$1005 cm^{-1}, 1155 cm^{-1} and 1525 cm^{-1}). Although the minimum of the negative signal aligns well with these GS frequencies, the broadening is significant, up to $\sim$100 cm^{-1}, making them much wider than the GS vibrational features. These signals can be observed even for carotenoids in cyclohexane, however dataset on Bcar, that is almost devoid of solvent and GS bleach signals confirms existence of the negative features most distinctly.

A second key characteristic of the S_2 state is the appearance of a broad positive band between 1500 and 1750 cm^{-1}. The precise position and shape of this feature varies only slightly among carotenoids except Lyc (Fig. 2(4A)) where it exhibits a significant redshift. For the shorter carotenoids; Neu (Fig. 2(1A)), Bcar (Fig. 2(2A)) and Spn (Fig. 2(3A)) a shoulder is discernible near 1700 cm^{-1} that overlaps well with the position of the main band of Lyc (Fig. 2(4A)). This observation suggests that the positive feature is, in fact, a superposition of two bands: one centered near 1600 cm^{-1} and another around 1700 cm^{-1}. As the conjugation length increases, the latter band grows in prominence and ultimately dominates the spectrum in Lyc (Fig. 2(4A)) even though in the longest carotenoid Spx (Fig. 2(5A)) the band is again comparable to what can be observed for shorter carotenoids. We assign the 1600 cm^{-1} band to the C=C stretching mode in the S_2 state. This is supported by the amplitude of this band in relation to carotenoid conjugation length. We clearly observe this band to decrease in amplitude with elongation of carotenoids. That is a natural consequence of resonance conditions. All carotenoids have S_2 state ESA in the near infrared region, typically peaking above 950 nm, but it shifts even further into lower energies for longer carotenoids.[13,15] With FSRS realized at 780 nm the pre-resonant conditions are strongest for shorter carotenoids and gradually decreasing for longer carotenoids whose S_2 state ESA is further in the near infrared region. It is possible that also the

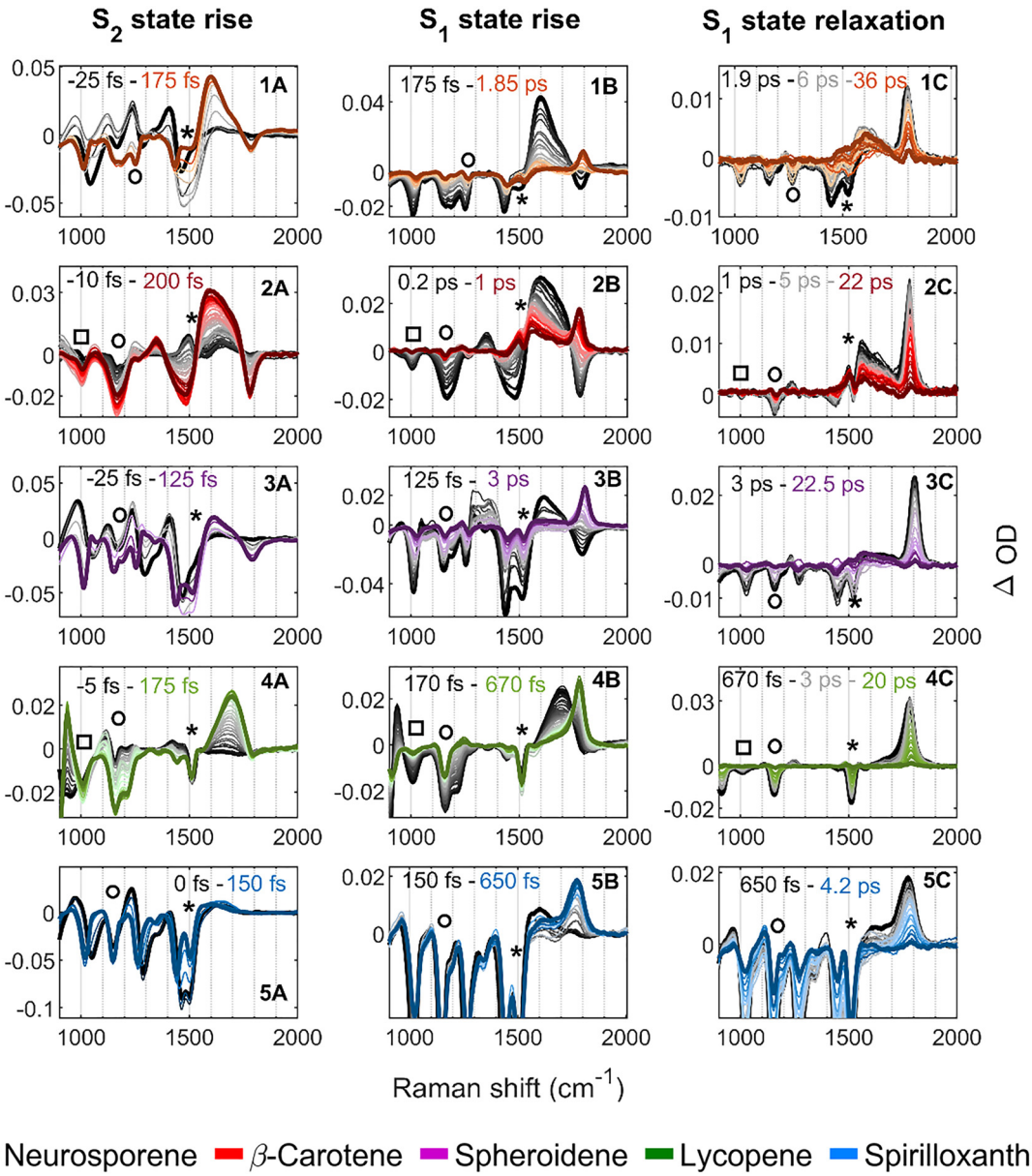

Fig. 2 Time-resolved spectra of all measured carotenoids. The first column shows the dynamics within the lifetime of the S_2 state, the second column shows the rise of the S_1 state, and the third column shows the relaxation of the S_1 state. The positions of carotenoid ground-state vibrations, all manifested as GS bleach, are marked in all panels. Asterisks indicate GS C=C stretching modes, circles mark GS C–C stretching modes. The methyl rocking GS vibration at approximately 1000 cm^{-1} is marked with a square, but only for lycopene and β-carotene. In all other cases, this band is overlapped by the ring deformation mode of the cyclohexane. All remaining vibrational bands are associated with the respective solvent.

1700 cm^{-1} band originate in C=C stretch of S_2 state. There is, however, a possibility that the 1700 cm^{-1} component originates from a vibrationally hot S_1 state that rapidly follows S_2 population. This hypothesis will be discussed in a later section. In Bcar measured in CCl_4, an additional weak positive band can be clearly identified near 1340 cm^{-1}, which we assign to the S_2 state C–C stretching vibration (Fig. 2(2A)). This assignment cannot be easily confirmed for carotenoids measured in cyclohexane due to interference with solvent signals in that region coupled with very small prominence of the band. Nevertheless, it is consistent with previous observations of the S_2 C–C mode in the orange carotenoid protein (OCP),[22] supporting its validity. After careful inspection similar small bands can be resolved at 1325 cm^{-1} in Lyc (Fig. 2(4A)), around 1360 cm^{-1} in Neu (Fig. 2(1A)) and Spn (Fig. 2(3A)) and around 1375 cm^{-1} in Spx (Fig. 2(5A)) most probably originating in C–C mode of the S_2 state as well.

A third characteristic of the S_2 response is a negative band that closely matches the known vibrational position of the S_1 state C=C stretching mode can be considered as a unique FSRS signature of the carotenoid S_1 state. It typically appears between 1770 and 1800 cm^{-1} for carotenoids in organic solvents and is always manifested as a positive peak. Although the negative dip

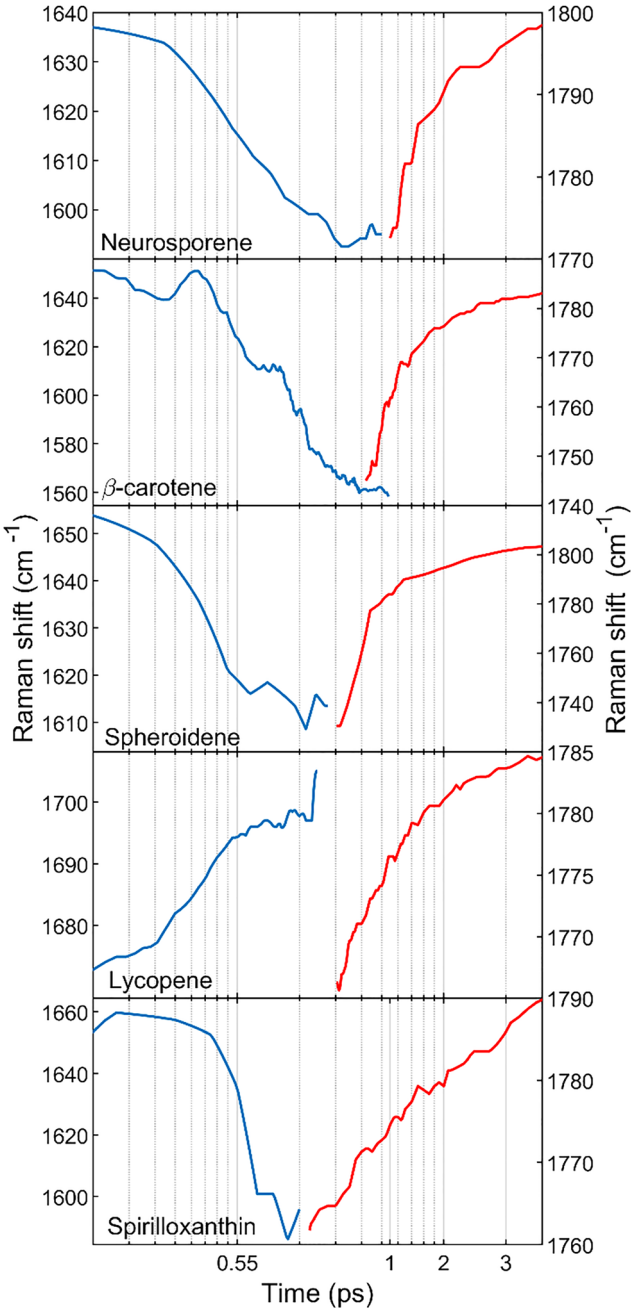

Fig. 3 Evolution of C=C mode frequency during S_2 (blue curves) and S_1 state (red curves) relaxation. The anomalous nature of S_2 peak shift trend in Lyc suggests that the band in fact represents cooling of hot-S_1 C=C mode.

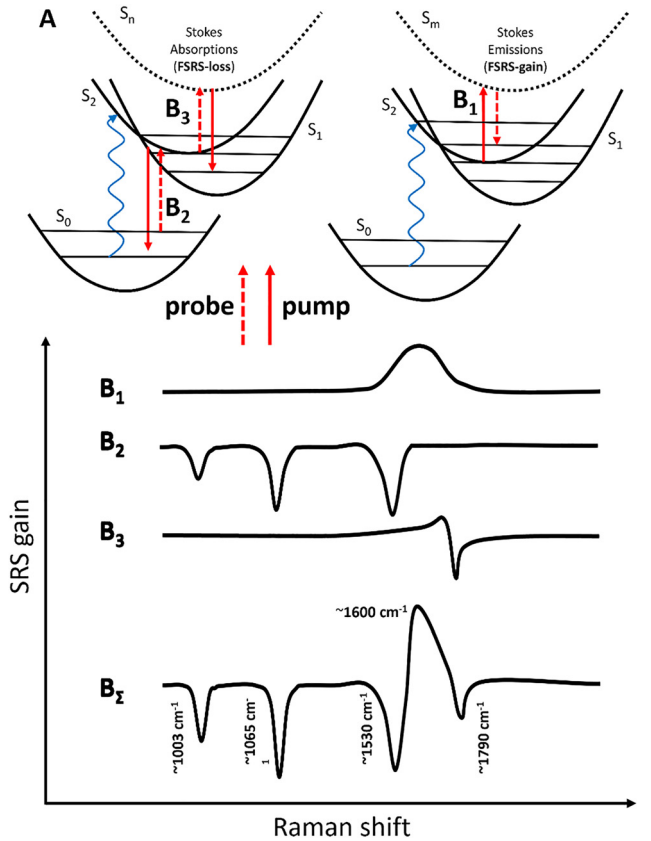

Fig. 4 Schematic of superposition forming the generic $1^1B_u^+$ state FSRS signature in near infrared resonance region, for simplicity only the dominant C=C stretch is visualized for excited states. (A) Diagram of FSRS processes involved in formation of FSRS signature. On the left there are processes that generate inverse signals (anti-Stokes scattering and resonance with SE) and on the right process generating positive signal *via* resonance with ESA. (B_1) $1^1B_u^+$ C=C vibration from resonance with ESA. (B_2) broadened GS signal from resonance with SE (B_3) inverse signature of $2^1A_g^-$ state from very-hot-S_1 state with positive band from hot mode and negative band form the relaxed mode (B_Σ) superposed generic signature of the $1^1B_u^+$ state when all key signals are present. Note that potential energy surfaces are drawn such that $2^1A_g^-$ state is close or slightly above $1^1B_u^+$ in GS configuration.

observed here at S_2 state population times does not perfectly match the peak position of the C=C band of a relaxed S_1 state, the spectral alignment is remarkably consistent across all carotenoids examined. This is clearly visible in the second column of Fig. 2, where the negative feature coincides with the eventual emergence of the S_1 peak at later time delays. Although the peak is not located at the same spectral position exactly, the strong correlation between its position at the S_2 and S_1 lifetimes suggests a functional connection between these features, making it unlikely that the observed negative signal is unrelated to S_1 state. The intensity of this (negative) signal varies between different carotenoids, and in Fig. 2(4B and 5B), we can see that after a certain conjugation length is exceeded, as in the case of Lyc (Fig. 2(4B)), the signal is no longer visible. However, this does not necessarily imply its absence: its detection may be obscured by the strong positive population signal near 1700 cm^{-1} observed in Lyc (Fig. 2(4B)). A detailed analysis was conducted to evaluate the possibility that this signal originated from S_1 population generated by the Rp pulse in the actinic pump-off configuration and thus to be an artifact of transient FSRS measurement. However, that is clearly not the case. As shown in SI, Fig. S1, the raw signals without subtraction of excitation-on and excitation-off conditions and any baseline treatment, clearly reveal a genuine signal inversion at the peak position in the actinic-on configuration at 180 fs,

while the actinic-off signal exhibits a flat baseline at the corresponding time delay. In contrast, a distinct positive signal appears at the S_1 state lifetime only in the actinic-on condition. These observations provide compelling evidence that the feature represents a genuine inverted (negative) signal associated with S_1 state C=C dynamics during S_2 state population times.

To summarize the observations, the time frame during which the S_2 state is populated is clearly associated with both positive and negative features. Positive signals are associated with C=C stretch manifested around 1600 cm^{-1} (values very mildly among individual carotenoids) and C–C stretch manifested around 1340 cm^{-1} (vary slightly more than C=C band), both partially enhanced by resonance with ESA of S_2 state in near infrared region. Additionally, there is shoulder at 1700 cm^{-1} whose origin is more difficult do decipher. In addition, there are broadened negative features at all GS mode locations and negative band at S_1 state C=C mode location. Whether all these signals directly originate from the S_2 state or involve additional secondary processes is a key issue addressed in this study. The relative proportion of positive and negative components varies substantially between carotenoids, although some broad trends with respect to conjugation length can be discerned. It is critical to emphasize that these features were recorded using a 780 nm Rp pulse, and any interpretation must consider context of resonances and pre-resonance at this wavelength. The S_2 state of carotenoids generally exhibits excited-state absorption in the near-infrared region, typically peaking above 950 nm. As such, a wavelength of 780 nm can generally be considered pre-resonant with S_2 ESA. However, the extent of pre-resonance is highly dependent on the specific carotenoid, as S_2 absorption tends to shift further into the red for longer carotenoids and generally becomes broader for more substituted carotenoids making relation to conjugated length carotenoid type specific.

S_1 state dynamics

In contrast to the S_2 state, the FSRS signature of the S_1 state is well established and the recorded results align with prior literature.[5–8] Our measurements reveal no major deviations from previously reported results. The dominant S_1 feature is a positive band near 1790 cm^{-1}, though its precise position differs slightly between carotenoids and does not show a straightforward correlation with conjugation length. However, this study highlights a previously underexplored aspect of S_1 state formation. As shown in the data, the rise of the S_1 signal does not immediately follow the decay of the S_2 signal—a phenomenon recorded in earlier studies but rarely addressed in detail.[19,36] Many prior FSRS investigations of carotenoids, mostly β-carotene, lacked sufficient temporal resolution or time sampling to unambiguously resolve the S_2 to S_1 transition, leading to sidelining this phenomenon. Our results show that the S_1 signal emerges with a noticeable delay, which coincides with the decay of the negative S_2 band (Fig. 2, middle section). As a result, at the S_2 half-life, the S_1 contribution is not yet fully developed; instead, it counterbalances the negative S_2 feature, resulting in a near-zero net signal. In the shortest carotenoids, Neu and Spn, this transition is marked by a brief plateau lasting several hundred femtoseconds. It can be observed in detail in Fig. S2 in the SI that compares the kinetics of C=C mode population at S_2 and S_1 frequencies. In longer carotenoids, where both S_2 and S_1 dynamics are faster, this transition appears smoother and the signal cancellation less distinct. Nevertheless, the consistent transition from a negative to a positive signal in the C=C stretching region is observed across all carotenoids studied under 780 nm FSRS probing and underscore its universal character. Another notable observation is a pronounced early-time downshift in the S_1 vibrational band. We attribute this to vibrational anharmonicity in the hot S_1 state, reflecting ongoing vibrational cooling. This relaxation process concludes within approximately 1.5 ps in the shortest carotenoids but is scarcely detectable in longer ones such as Spx.

System relaxation

The S_1 state dynamics is characterized by a C=C stretch around 1790 cm^{-1}, decaying with a lifetime consistent with S_1 state relaxation known from literature.[5–7] In the case of Bcar in CCl_4, an additional broad band spanning 1450–1750 cm^{-1}, peaking near 1550 cm^{-1}, is observed (Fig. 2(2C)). This feature is tentatively assigned to an intramolecular charge transfer (ICT) state based on previous reports of similar features,[37] which forms despite the absence of a keto group and is likely due to the properties of CCl_4. Although the solvent is globally nonpolar owing to its symmetric tetrahedral structure, the individual C–Cl bonds are strongly polar. Interactions with these bonds may induce local asymmetry in a fraction of carotenoid molecules, promoting ICT state formation. Previous studies have shown that ICT features are particularly prominent when probed in the red or near infrared region, due to the ICT state's red-shifted absorption resonating more strongly with near-IR excitation compared to both S_1 and S_2 state.[37] The fact that the ICT signal reaches only about half the amplitude of the S_1 peak despite the strong resonance suggests that the actual population of the ICT state is relatively small.

Evolution of C=C stretch energy

The temporal evolution of the peak maximum frequency was obtained by directly reading the peak positions from densely sampled FSRS datasets and is presented in Fig. 3. It illustrates the instantaneous vibrational frequency of the C=C stretching mode associated with the S_2 state (within the 1500–1750 cm^{-1} region) and the S_1 state (within the 1750–1850 cm^{-1} region) for photoexcited carotenoids. The data reveal a distinct blue shift in the C=C stretching frequency during the lifetime of the S_2 state, suggesting structural relaxation along the reaction coordinate. This is followed by a transition through a conical intersection into the S_1 state, where the C=C stretching frequency exhibits a blue shift as it approaches its final value. This upward shift reflects vibrational cooling within the S_1 state and likely also continued evolution of the underlying potential energy surface, which increases the energy separation between the S_2 and S_1 states during early stages of relaxation.

Notably, Lyc shows an anomalously small frequency difference between its S_2 and S_1 C=C stretching modes. This behavior is attributed to Lyc's high molecular symmetry and minimal end-group substitution. As will be discussed in more detail later, it is possible that the C=C band FSRS signature recorded during Lyc's nominal S_2 lifetime primarily originates from a vibrationally hot S_1 state rather than from S_2. This interpretation is supported by the observation that, unlike other carotenoids—where the S_2 C=C band shifts toward lower frequencies, the corresponding feature in Lyc shifts toward higher frequencies, a trend clearly associated with the cooling dynamics of the S_1 state. Lyc nominally has the second most red-shifted absorption for both the S_1 and S_2 states (*i.e.*, absorption to S_n), making the 780 nm region arguably less resonant with S_2, since the $S_2 \rightarrow S_n$ absorption shifts further into the infrared, away from 780 nm. Conversely, it may be more resonant with the $S_1 \rightarrow S_n$ transition, and in particular with the hot-$S_1 \rightarrow S_n$ transition, which has an absorption tail extending into the near-infrared region, effectively bringing it closer to 780 nm.[23] In the case of the longest carotenoid with the most red-shifted resonances, Spx, we observe a very weak S_2-state signature, which is consistent with the presented theory that pre-resonance diminishes with increasing conjugation length. However, the S_2-state signature appears to be located similarly to that of shorter carotenoids, that means around 1600 cm^{-1} and the hot-S_1 signature is not clearly manifested, making the S_2 state of Lyc dynamics somewhat anomalous compared to all other recorded carotenoids.

Kinetics of C=C modes

In Fig. S7 of the SI, a simple kinetic analysis of the bands associated with the C=C stretching modes of the S_1 and S_2 states is presented. The results of this analysis are summarized in Table 1. While a detailed study of kinetic parameters is not the primary aim of this work, it can be noted that the Raman signature of the S_1 state C=C mode closely follows the well-established S_1 state lifetime. In contrast, the decay of the S_2 state C=C mode differs significantly from reported S_2 state lifetimes as it is generally shorter than those obtained from fluorescence upconversion measurements. This discrepancy likely arises from the very rapid vibronic and electronic reorganization within the early S_2 state, which generates ultrafast dynamics in S_2 resonance. Specifically, the hot S_2 state is believed to be considerably more resonant with the Rp pulse at 780 nm than the relaxed S_2 state, and it is likely that the Raman cross section evolves rapidly, as the polarizability can also be affected by nuclear rearrangements. Consequently, the kinetics extracted from the S_2 Raman signatures are convoluted with rapid S_2 state cooling and conformational stabilization processes. Additionally, the hot S_1 state signatures partially overlap with the S_2 state signatures, resulting in distinctly bi-exponential kinetics recorded at 1600 cm^{-1}: the fast component primarily originates from the S_2 state, while the slower component arises predominantly from the hot S_1 state.

Table 1 Kinetic constants were derived from the temporal evolution of the C=C mode of the S_2 state at 1600 cm^{-1} and the C=C mode of the S_1 state at 1780 cm^{-1}. The S_2 mode generally displays strongly bi-exponential behavior, likely due to the overlap between the S_2 state lifetime and the cooling dynamics of the hot S_1 state

	S_2 C=C at 1600 cm^{-1}		S_1 C=C at 1780 cm^{-1}
Carotenoid	τ_1 [ps]	τ_2 [ps]	τ [ps]
Neurosporene	0.12 ± 0.02	0.57 ± 0.28	29.0 ± 1.9
β-Carotene	0.13 ± 0.01	2.25 ± 0.28	11.2 ± 0.4
Spheroidene	0.07 ± 0.01	—	5.93 ± 0.28
Lycopene	0.04 ± 0.003	0.60 ± 0.015	4.27 ± 0.11
Spirilloxanthin	0.90 ± 0.66	—	1.02 ± 0.09

Discussion

Multi component nature of S_2 state signature and origin of negative signals

Before a detailed discussion about the assignment of the observed signals, it is important to single out the sources of confusion that complicate any assignment of the S_2 state signature. The challenges associated with recording and assigning the vibrational signature of the S_2 state are affected by several key issues; baseline correction artifacts, misinterpretation of negative signals, particularly in proximity to solvent bands, insufficient temporal resolution and sampling, inadequate spectral resolution and fundamental inseparability of certain signals that might have a different origin. All these features compromised capacity to properly separate positive and negative signals and thus set a genuine baseline for S_2 state signature.

Baseline correction remains a persistent challenge in FSRS spectroscopy and is arguably one of the primary factors limiting its broad adoption relative to mid-infrared vibrational spectroscopy. Most baseline correction methods rely on threshold criteria that define the maximum width of features considered as true spectral peaks. In the simplest way it is for example the order of polynomial used to fit the baseline, but other approaches have this parameter indirectly as well, *e.g.* in the case of machine learning based methods the widths of peaks generated in the training set. The C=C stretch associated with the S_2 state is characteristically broad, and standard methods optimized for narrower features, such as those observed for the ground state or the S_1 state, tend to misclassify this broad feature as part of the baseline. To address this, we systematically tested multiple baseline correction approaches. Despite methodological differences, all consistently revealed the presence of the broad feature attributed to the S_2 state, supporting its authenticity. Furthermore, recent work[9] summarizing S_1 state signatures in various carotenoids includes, in the SI, FSRS data from early pump probe delays. These data also exhibit the same spectral features identified in our study, even though no effort was made in that work to optimize baseline correction for their extraction and so further reinforce the validity of our assignment. The other baseline related topic is removal of the GS bleach. While in TA and mid-IR spectroscopy negative signals arising from GS bleach are standard and

well-understood, FSRS has historically adopted a different methodological approach. Specifically, GS vibrational peaks are often carefully removed by linearly scaling and subtracting a GS reference spectrum.[5,7,19] This practice is partly justified, as excited-state FSRS spectra are typically recorded under distinct resonance conditions, and the intensity of GS bleach signals is generally less informative compared to TA or mid-infrared data. Furthermore, the presence of a spurious GS bleach, which often arise from experimental artifacts, compromises the reliability of bleach amplitudes as indicators of excited-state population. However, this routine suppression of negative signals can obscure genuine spectral features. Notably, negative bands especially when coinciding with GS vibrational modes and even the S_1 state signatures can in fact be authentic components of the S_2 state vibrational signature and that is the claim to be justified in this work. In case of the S_2 state the negative features are not artifacts resulting from the subtraction of a GS reference spectrum. This becomes more prominent with narrowing the Rp pulse, making GS bleach and negative GS signal associated with the S_2 state more distinguishable by genuine GS bleach being much narrower than negative S_2 features that follow the broad bandwidth dictated by short S_2 state lifetime. Since FSRS is a nonlinear process, its efficiency drops with increased pulse duration. Old experiments were conducted with relatively broad Rp pulses that made the negative signal from S_2 state less distinctly broader than GS modes that were broadened by instrument spectral resolution below their intrinsic bandwidth.[19,38,39]

The appearance of such negative features raises a fundamental question regarding their physical origin, which is addressed in the following section. In FSRS spectroscopy, negative vibrational signals can arise from two principal mechanisms, and due to the complex nature of the S_2 state, it remains challenging to determine the dominant contributor with complete certainty. One plausible explanation involves resonance with SE, which can produce inverted (negative) peaks in the Stokes (red shifted) region of the FSRS spectrum.[26,28] It is well-established that the S_2 state exhibits a broad SE band, spanning from the blue to the red region of the spectrum. Although up-conversion measurements indicate that this emission does not extend to 800 nm,[40] FSRS is highly sensitive to even pre-resonant conditions, which can substantially influence the observed spectral response.

The spectral distribution of SE, characterized by an exponential decline from the blue-green to the red, suggests that the Rp pulse is more closely pre-resonant with SE than the Stokes component of the probe pulse at around 925 nm for 1700 cm^{-1} Stokes shift. Under these conditions, the conventional off-resonant FSRS interaction, in which the Rp pulse is absorbed and the probe experiences gain, can be inverted so that the Rp pulse undergoes amplification, while the probe experiences attenuation due to absorption. Theoretical work has supported the feasibility of such signal inversion when SE resonance is present,[26,28] although experimental verification under realistic conditions remains limited. Importantly, resonance conditions not only enhance signal intensity but can also induce vibrational coherence at states accessed by resonance. Indeed, resonant Raman scattering has historically been used to predict ultrafast dynamics in retinal systems prior to the development of femtosecond time-resolved methods.[41] Those phenomena are applicable to resonance with SE as well, albeit with an inverted sign. In this context, resonance with SE from the excited S_2 state to the ground state effectively couples to ground-state vibrational modes, thereby incorporating them into the observed S_2 state spectral signature. However, since SE arises from the short-lived S_2 state, the associated vibrational features appear significantly broadened due to the finite lifetime of the mediating electronic state. This interpretation provides a plausible explanation for negative peaks observed at spectral positions corresponding to GS vibrational modes. However, it fails to account for the negative feature observed at 1790 cm^{-1}, as SE from the S_2 to the S_1 transition is negligible. An alternative mechanism for peak reversal is the inversion of vibrational population. Several studies have proposed that the energy gap between the S_2 and S_1 states is significantly reduced in the relaxed ground-state geometry, or that the S_1 state may even lie above the S_2 state at GS nuclear coordinates.[42] It is, therefore, likely that the initially formed S_1 state is internally hot and formed exquisitely at vibrationally excited state. Under such conditions, the lowest vibrational levels of the early formed S_1 state may be populated primarily through an anti-Stokes process, wherein the optical field and probe side gains energy from the molecule rather than depositing it. In this context, we propose that the observed inversion of the S_1 C═C stretch band at S_2 state population times is a manifestation of a genuine anti-Stokes Raman process at the low energy (traditionally called Stokes) side of FSRS signals. This interpretation predicts a comparable impact on both low and high energy side signals, as it does not rely directly on molecular resonance effects. That aligns with the high energy side FSRS spectra of Lyc in a recent report[23] where the negative peak can be seen as well. In this context we speculate that the negative signal at 1790 cm^{-1} does not originate in resonance with simulated emission but in a hot-S_1 state that exists in the form of population inversion (excited S_1 modes are occupied more than relaxed S_1 modes).

It is worth noting that all mentioned spectral features associated with S_2 state, both positive and negative, are in fact resolvable in the seminal work by Kukura *et al.*[21] and later reproduced by Redeckas *et al.*,[43] although in both works signals were from current perspective somewhat modulated by baseline treatment procedures. Interestingly, the work[43] more clearly manifests the negative feature at S_1 peak location during the S_2 state lifetime, and to a large extend it is intermediate between interpretation by Kukura *et al.*[21] and the one presented in this work. In this regard, the present work in fact supports the validity of the oldest published S_2 state FSRS signature proposed in another work by Kukura *et al.*[38] The key advancement offered here is the reinterpretation of the features in a correctly placed baseline. Three broad bands were identified in those studies. This work suggests that the S_2 state signature in fact primarily consists of 3 broad negative signals. These valleys are likely the result of pre-resonance with SE from the S_2 state into the ground state, contributing to the complex structure of

the S_2 signature when probed with a 780 nm (or similar) Raman pulse.

In two previous studies by Takaya *et al.*,[6,44] FSRS measurements of β-carotene revealed a broad positive S_2-associated band centered around 1600 cm^{-1}. The absence of a negative S_1-related feature can likely be attributed to different resonance conditions, as the Raman pump wavelength was set to 1190 nm that nearly perfectly resonates with the S_2 state.[6,44] In the given context we consider those works as the most accurate assignments of genuine S_2 Raman signatures.

A necessary point of discussion concerns the discrepancies between other previously published studies on this topic. In particular, the work[45] presents a comparison of FSRS data for Bcar collected using Rp wavelengths of 776 nm (FSRS analyzed on the high energy side) and 573 nm (FSRS analyzed on the low side). The spectra recorded at 776 nm exhibit features that are in qualitative agreement with the results presented in the current study. However, the comparison is difficult due to effects inherent to high energy side anti-Stokes (blue side) region, where resonance with ESA leads not only to signal enhancement but also to peak shape distortion but even to peak reversal.[26] In contrast, the data acquired at 573 nm do not display the broad positive band; instead, they show only the negative peak associated with the S_1 state and GS.[45] This observation can be rationalized by considering the resonance conditions: at 573 nm, the experiment is no longer resonant with ESA from the S_2 state, thereby suppressing its spectral contribution. Simultaneously, the resonance with the S_1 state, particularly the hot-S_1 state, is enhanced together with resonance with SE, leading to the more prominent appearance of its vibrational signature in the FSRS data. In short it seems that at shorter wavelengths of Rp pulse, specifically in the visible region, the negative S_1 peak around 1790 cm^{-1} becomes more prominent while in near infrared resonance with S_2 the positive peak at 1600 cm^{-1} becomes more prominent. Underscoring their separate origin from S_1–S_n and S_2–S_m resonances respectively.

Two phase S_1 state cooling and its implication to S_x state

The so-called S_x state was originally proposed to account for discrepancies observed in TA data during the conversion from the S_2 to the S_1 electronic state.[46–48] These inconsistencies were further underscored by FSRS measurements, which revealed a distinct delay in the appearance of the S_1 associated C=C stretching mode, a delay that does not temporally coincide with the decay of the S_2 state population.[40] The data presented herein offer a plausible mechanistic explanation for this observation. Specifically, because the S_2 state is characterized by an inverted peak at the spectral position of the S_1 C=C stretch mode, during the intermediate phase of the S_2 to S_1 population transfer, when both states are concurrently populated and the opposing contributions from these two states effectively cancel each other and result in a transient plateau in the spectral signal. This effect is particularly pronounced with the shorter carotenoids, Spn and Neu, as illustrated in Fig. S2 in SI. Consequently, the C=C stretching band associated with the relaxed S_1 state does not emerge concurrently with S_2 depopulation but instead appears during its trailing phase. We propose that this temporal offset arises from a biphasic vibrational relaxation process within the S_1 state. The depopulation of the S_2 state is ultrafast and marked by strong coupling between electronic and vibration states. During the initial phase of S_2 decay, the S_1 state is populated in a highly excited configuration (here referred to as "very-hot-S_1"), likely exhibiting vibrational population inversion in which only the high-energy vibrational levels are significantly occupied. At this stage, the lowest-energy vibrational level of the C=C stretch mode in the S_1 state ($\sim$1790 cm^{-1}) remains unpopulated, while the higher, populated vibrational levels are shifted closer to 1700 cm^{-1} due to anharmonicity. Consequently, this mode can only be accessed *via* anti-Stokes Raman scattering, resulting in an inverted (negative) feature in the FSRS spectrum. In contrast, the very-hot-S_1 state gives rise to strong positive spectral features near 1700 cm^{-1}, originating from anharmonically shifted vibrationally excited modes, and tends to spectrally overlap with the S_2-related vibrational modes near 1600 cm^{-1}. Notably, the S_1 associated C–C stretching mode near 1240 cm^{-1} is also observed in the data at S_2 state times, yet it does not exhibit signs of vibrational inversion and appears as a positive band in the FSRS spectra at particularly early S_2 state lifetimes, akin to the relaxed S_1 state. This observation supports the hypothesis that the transition from the GS to the S_2 state induces a rapid bond-length reorganization that disproportionately affects double and single bonds, channeling vibrational energy preferentially into the C=C modes. This interpretation is consistent with the relatively moderate upshift of the C–C mode in S_1 state (approximately 80 cm^{-1}) compared to the significantly larger shift observed for the C=C mode (approaching 1700 cm^{-1}). Thus, the observation of a sign inversion in the C=C mode while not present in the C–C mode may represent the first experimental indication of such bond-specific vibrational population dynamics. The very-hot-S_1 population rapidly relaxes into a hot-S_1 state, in which C=C stretch modes remain excited but begin to approach Boltzmann distribution, with lower-energy modes already predominantly occupied. Although vibrational cooling within the S_1 state typically occurs on the order of several hundred femtoseconds, the vibrational inversion associated with the very-hot-S_1 state is likely even more short-lived, potentially shorter than the lifetime of the S_2 state and rendering it kinetically inseparable from S_2 in standard global analysis models. That is in alignment with picosecond spontaneous Raman experiments that did not record anti-Stokes signal of the S_1 state.[10] The vibrationally excited S_1 is arguably even shorter lived and less populated then S_2 state making it impossible to capture without femtosecond techniques. In this context, we propose that certain spectral features previously attributed to the S_x state may instead arise from this intermediate phase, wherein the S_1 state is still in a vibrationally inverted, non-equilibrium configuration that more closely follows the decay of the S_2 state rather than the dynamics of the fully relaxed S_1 state. This transient and highly non-equilibrium S_1 population exhibits distinct spectral characteristics and dynamic behavior that deviate significantly from the canonical

S_1 fingerprint, supporting the interpretation that the so-called S_x state may, in fact, be a manifestation of vibrational inversion during the early relaxation pathway of the S_1 state on its potential energy surface that we call here a very-hot-S_1 state.

Conclusion

We observed a Raman signature corresponding to the S_2 ($1^1B_u^+$) state of carotenoids, characterized by a prominent C=C stretching mode, appearing as a broad ($\sim$100 cm^{-1}) band centered near 1600 cm^{-1}. In addition, the S_2 state exhibits a weaker band around 1350 cm^{-1}, which is likely attributable to a C–C stretching vibration. However, those positive spectral signatures are in general obscured by overlapping features that are kinetically indistinguishable from the S_2 population. These overlapping signals likely arise from two primary sources: SE from the S_2 state and contributions from the very-hot-S_1 state, that is formed predominantly during the early phase of S_2 population. SE manifests as ground-state-like C=C and C–C stretch and methyl rock bands, but these are broadened due to the short lifetime of the S_2 state and exhibit inverted signs. This inversion arises because SE couples to the Rp and Pr fields in the opposite phase relative to excited-state absorption. The very-hot-S_1 state contributes a distinct positive band near 1700 cm^{-1} and a negative band around 1790 cm^{-1}. This structure likely originates from a transient vibrational population inversion of the C=C stretching mode during the initial formation of the S_1 state, in which only the highly excited vibrational levels are populated. That is visualized in Fig. 4. Interestingly, the C–C stretching mode associated with the very-hot-S_1 state also appears in the FSRS spectrum; however, unlike the C=C mode, it does not show evidence of population inversion and presents as a positive band similar to that observed in the relaxed S_1 state. This difference may reflect rapid bond-length reorganization following the GS to S_2 electronic transition, which appears to affect the C–C and C=C bonds in an uneven way. Taken together, these observations suggest that some of the spectral and kinetic features previously attributed to the so-called S_x state may, in fact, originate from the temporal overlap between the S_2 state and the very-hot-S_1 state. The latter exists in a strongly vibrationally inverted configuration and thus exhibits markedly different spectral characteristics from the thermally relaxed S_1 state.

Conflicts of interest

There are no conflicts to declare.

Data availability

The data supporting this article have been included as part of the SI. Supplementary information contains supplementary figures and complete experimental data. See DOI: **https://doi.org/10.1039/d5cp02711j**.

Acknowledgements

TP thanks the Czech Science Foundation, grant 24-11344S, for financial support. MK thanks the Czech Science Foundation, grant 21-09692M and Johannes Amos Comenius Operational Programme OPJAK (project No. SENDISO-CZ.02.01.01/00/22_008/0004596), for financial support.

References

1 M. M. Mendes-Pinto, E. Sansiaume, H. Hashimoto, A. A. Pascal, A. Gall and B. Robert, Electronic absorption and ground state structure of carotenoid molecules, *J. Phys. Chem. B*, 2013, **117**, 11015–11021.
2 P. Tavan and K. Schulten, Electronic excitations in finite and infinite polyenes, *Phys. Rev. B: Condens. Matter Mater. Phys.*, 1987, **36**, 4337–4358.
3 T. Noguchi, H. Hayashi, M. Tasumi and G. H. Atkinson, Frequencies of the Franck-Condon active ag C = C stretching mode in the 2 1Ag- excited state of carotenoids, *Chem. Phys. Lett.*, 1990, **175**, 163–169.
4 H. Hashimoto and Y. Koyama, Raman spectra of all-trans-β-carotene in the S1 and T1 states produced by direct photoexcitation, *Chem. Phys. Lett.*, 1989, **163**, 251–256.
5 M. Quick, M. A. Kasper, C. Richter, R. Mahrwald, A. L. Dobryakov, S. A. Kovalenko and N. P. Ernsting, β-carotene revisited by transient absorption and stimulated Raman spectroscopy, *ChemPhysChem*, 2015, **16**, 3824–3835.
6 T. Takaya, M. Anan and K. Iwata, Vibrational relaxation dynamics of β-carotene and its derivatives with substituents on terminal rings in electronically excited states as studied by femtosecond time-resolved stimulated Raman spectroscopy in the near-IR region, *Phys. Chem. Chem. Phys.*, 2018, **20**, 3320–3327.
7 P. Kukura, D. W. McCamant and R. A. Mathies, Femtosecond time-resolved stimulated Raman spectroscopy of the S2 (1Bu +) excited state of β-carotene, *J. Phys. Chem. A*, 2004, **108**, 5921–5925.
8 H. Hashimoto and Y. Koyama, The C = C stretching Raman lines of β-carotene isomers in the S1 state as detected by pump-probe resonance Raman spectroscopy, *Chem. Phys. Lett.*, 1989, **154**, 321–325.
9 I. Šímová, P. Chrupková, A. T. Gardiner, M. Koblížek, M. Kloz and T. Polívka, Femtosecond stimulated Raman spectroscopy of linear carotenoids, *J. Phys. Chem. Lett.*, 2024, **15**, 7466–7472.
10 D. W. McCamant, J. E. Kim and R. A. Mathies, Vibrational relaxation in β-carotene probed by picosecond Stokes and anti-Stokes resonance Raman spectroscopy, *J. Phys. Chem. A*, 2002, **106**, 6030–6038.
11 T. Polívka and V. Sundström, Ultrafast dynamics of carotenoid excited states- from solution to natural and artificial systems, *Chem. Rev.*, 2004, **104**, 2021–2071.
12 A. N. Macpherson and T. Gillbro, Solvent dependence of the ultrafast S2 −S1 internal conversion rate of β-carotene, *J. Phys. Chem. A*, 1998, **102**, 5049–5058.

13 D. Niedzwiedzki, J. F. Koscielecki, H. Cong, J. O. Sullivan, G. N. Gibson, R. R. Birge and H. A. Frank, Ultrafast dynamics and excited state spectra of open-chain carotenoids at room and low temperatures, *J. Phys. Chem. B*, 2007, **111**, 5984–5998.
14 D. Kosumi, K. Yanagi, R. Fujii, H. Hashimoto and M. Yoshizawa, Conjugation length dependence of relaxation kinetics in β-carotene homologs probed by femtosecond Kerr-gate fluorescence spectroscopy, *Chem. Phys. Lett.*, 2006, **425**, 66–70.
15 D. Kosumi, M. Fujiwara, R. Fujii, R. J. Cogdell, H. Hashimoto and M. Yoshizawa, The dependence of the ultrafast relaxation kinetics of the S2 and S1 states in β-carotene homologs and lycopene on conjugation length studied by femtosecond time-resolved absorption and Kerr-gate fluorescence spectroscopies, *J. Chem. Phys.*, 2009, **130**, 214506.
16 A. P. Shreve, J. K. Trautman, T. G. Owens and A. C. Albrecht, Determination of the S2 lifetime of β-carotene, *Chem. Phys. Lett.*, 1991, **178**, 89–96.
17 M. Yoshizawa and M. Kurosawa, Femtosecond time-resolved Raman spectroscopy using stimulated Raman scattering, *Phys. Rev. A: At., Mol., Opt. Phys.*, 1999, **61**, 013808.
18 T. Buckup, J. Hauer, J. MÖhring and M. Motzkus, in *Ultrafast Phenomena XVI*, ed A. W. Castleman, J. P. Toennies, K. Yamanouchi and W. Zinth, Springer, Berlin Heidelberg, 2009, vol. 92, pp. 442–444.
19 D. W. McCamant, P. Kukura and R. A. Mathies, Femtosecond time-resolved stimulated Raman spectroscopy: Application to the ultrafast internal conversion in β-carotene, *J. Phys. Chem. A*, 2003, **107**, 8208–8214.
20 T. Polívka, S. Kaligotla, P. Chábera and H. A. Frank, An intramolecular charge transfer state of carbonyl carotenoids: Implications for excited state dynamics of apocarotenals and retinal, *Phys. Chem. Chem. Phys.*, 2011, **13**, 10787–10796.
21 P. Kukura, D. W. McCamant and R. A. Mathies, Femtosecond stimulated Raman spectroscopy, *Annu. Rev. Phys. Chem.*, 2007, **58**, 461–488.
22 P. Chrupková, I. H. M. van Stokkum, T. Friedrich, M. Moldenhauer, N. Budisa, H.-W. Tseng, T. Polívka, D. A. Cherepanov, E. G. Maksimov and M. Kloz, Raman vibrational signatures of excited states of echinenone in the orange carotenoid protein (OCP) and implications for its photoactivation mechanism, *J. Mol. Biol.*, 2024, **436**, 168625.
23 I. H. M. van Stokkum, J. J. Snellenburg, P. Chrupková, J. Dostal, S. Weigand, J. Weißenborn, J. T. M. Kennis and M. Kloz, Target analysis resolves the ground and excited state properties from femtosecond stimulated Raman spectra, *J. Phys. Chem. Lett.*, 2024, **15**, 9397–9404.
24 G. Batignani, G. Fumero, E. Pontecorvo, C. Ferrante, S. Mukamel and T. Scopigno, Genuine dynamics vs cross phase modulation artifacts in femtosecond stimulated Raman spectroscopy, *ACS Photonics*, 2019, **6**, 492–500.
25 D. W. McCamant, Re-evaluation of rhodopsin's relaxation kinetics determined from femtosecond stimulated Raman lineshapes, *J. Phys. Chem. B*, 2011, **115**, 9299–9305.
26 G. Batignani, E. Pontecorvo, G. Giovannetti, C. Ferrante, G. Fumero and T. Scopigno, Electronic resonances in broadband stimulated Raman spectroscopy, *Sci. Rep.*, 2016, **6**, 18445.
27 G. Batignani, C. Ferrante and T. Scopigno, Accessing excited state molecular vibrations by femtosecond stimulated Raman spectroscopy, *J. Phys. Chem. Lett.*, 2020, **11**, 7805–7813.
28 G. Batignani, C. Ferrante, G. Fumero, M. Martinati and T. Scopigno, Femtosecond stimulated Raman spectroscopy, *Nat. Rev. Methods Primers*, 2024, **4**, 34.
29 T. Khan, R. Litvín, V. Šebelík and T. Polívka, Excited-state evolution of keto-carotenoids after excess energy excitation in the UV region, *ChemPhysChem*, 2021, **22**, 471–480.
30 M. T. Gebrekidan, C. Knipfer and A. S. Braeuer, Refinement of spectra using a deep neural network: Fully automated removal of noise and background, *J. Raman Spectrosc.*, 2021, **52**, 723–736.
31 M. Kloz, R. van Grondelle and J. T. M. Kennis, Correction for the time dependent inner filter effect caused by transient absorption in femtosecond stimulated Raman experiment, *Chem. Phys. Lett.*, 2012, **544**, 94–101.
32 M. Kloz, R. van Grondelle and J. T. M. Kennis, Wavelength-modulated femtosecond stimulated Raman spectroscopy – approach towards automatic data processing, *Phys. Chem. Chem. Phys.*, 2011, **13**, 18123–18133.
33 E. Papagiannakis, I. H. M. van Stokkum, R. van Grondelle, R. A. Niederman, D. Zigmantas, V. Sundström and T. Polívka, A near-infrared transient absorption study of the excited-state dynamics of the carotenoid spirilloxanthin in solution and in the LH1 complex of Rhodospirillum rubrum, *J. Phys. Chem. B*, 2003, **107**, 11216–11223.
34 V. Chynwat and H. A. Frank, The application of the energy gap law to the S1 energies and dynamics of carotenoids, *Chem. Phys.*, 1995, **194**, 237–244.
35 H. A. Frank, V. Chynwat, R. Z. B. Desamero, R. Farhoosh, J. Erickson and J. Bautista, On the photophysics and photochemical properties of carotenoids and their role as light-harvesting pigments in photosynthesis, *Pure Appl. Chem.*, 1997, **69**, 2117–2124.
36 M. Kloz, S. Pillai, G. Kodis, D. Gust, T. A. Moore, A. L. Moore, R. van Grondelle and J. T. M. Kennis, Carotenoid photoprotection in artificial photosynthetic antennas, *J. Am. Chem. Soc.*, 2011, **133**, 7007–7015.
37 K. Redeckas, V. Voiciuk and M. Vengris, Investigation of the S1/ICT equilibrium in fucoxanthin by ultrafast pump–dump–probe and femtosecond stimulated Raman scattering spectroscopy, *Photosynth. Res.*, 2016, **128**, 169–181.
38 P. Kukura, R. Mathies and D. W. McCamant, Femtosecond broadband stimulated Raman: A new approach for high-performance vibrational spectroscopy, *Appl. Spectrosc.*, 2003, **57**, 1317–1323.
39 D. W. McCamant, P. Kukura, S. Yoon and R. A. Mathies, Femtosecond broadband stimulated Raman spectroscopy: Apparatus and methods, *Rev. Sci. Instrum.*, 2004, **75**, 4971–4980.
40 H. Kandori, H. Sasabe and M. Mimuro, Direct determination of a lifetime of the S2 state of β-carotene by

femtosecond time-resolved fluorescence spectroscopy, *J. Am. Chem. Soc.*, 1994, **116**, 2671–2672.

41 R. Mathies, T. B. Freedman and L. Stryer, Resonance Raman studies of the conformation of retinal in rhodopsin and isorhodopsin, *J. Mol. Biol.*, 1977, **109**, 367–372.

42 E. J. Taffet, B. G. Lee, Z. S. D. Toa, N. Pace, G. Rumbles, J. Southall, R. J. Cogdell and G. D. Scholes, Carotenoid nuclear reorganization and interplay of bright and dark excited states, *J. Phys. Chem. B*, 2019, **123**, 8628–8643.

43 K. Redeckas, V. Voiciuk and M. Vengris, A tunable femtosecond stimulated Raman scattering system based on spectrally narrowed second harmonic generation, *Lith. J. Phys.*, 2016, **56**, 21–34.

44 T. Takaya and K. Iwata, Relaxation mechanism of β-carotene from S2 ($1Bu^+$) state to S1 ($2Ag^-$) state: Femtosecond time-resolved near-IR absorption and stimulated resonance Raman studies in 900–1550 nm region, *J. Phys. Chem. A*, 2014, **118**, 4071–4078.

45 M. Quick, A. L. Dobryakov, S. A. Kovalenko and N. P. Ernsting, Resonance femtosecond-stimulated Raman spectroscopy without actinic excitation showing low-frequency vibrational activity in the S2 state of all-trans β-carotene, *J. Phys. Chem. Lett.*, 2015, **6**, 1216–1220.

46 W. F. Beck, M. M. Bishop, J. D. Roscioli, S. Ghosh and H. A. Frank, Excited state conformational dynamics in carotenoids: Dark intermediates and excitation energy transfer, *Arch. Biochem. Biophys.*, 2015, **572**, 175–183.

47 D. Accomasso, S. Arslancan, L. Cupellini, G. Granucci and B. Mennucci, Ultrafast excited-state dynamics of carotenoids and the role of the Sx state, *J. Phys. Chem. Lett.*, 2022, **13**, 6762–6769.

48 T. M. N. Mohan, C. H. Leslie, S. Sil, J. B. Rose, R. W. Tilluck and W. F. Beck, Broadband 2DES detection of vibrational coherence in the Sx state of canthaxanthin, *J. Chem. Phys.*, 2021, **155**, 035103.